Hydrology Research

A practical methodology to perform global sensitivity analysis for 2D hydrodynamic computationally intensive simulations

Saba Mirza Alipour [iD][a,*], Kolbjørn Engeland[b] and Joao Leal[a]

[a] Department of Engineering and Science, University of Agder, Jon Lilletuns vei 9, 4879 Grimstad, Norway
[b] Norwegian Water Resources and Energy Directorate (NVE), P.O. Box 5091 Maj., 0301 Oslo, Norway
*Corresponding author. E-mail: saba.m.alipour@uia.no

[iD] SMA, 0000-0003-2078-3703

ABSTRACT

Sensitivity analysis is a commonly used technique in hydrological modeling for different purposes, including identifying the influential parameters and ranking them. This paper proposes a simplified sensitivity analysis approach by applying the Taguchi design and the ANOVA technique to 2D hydrodynamic flood simulations, which are computationally intensive. This approach offers an effective and practical way to rank the influencing parameters, quantify the contribution of each parameter to the variability of the outputs, and investigate the possible interaction between the input parameters. A number of 2D flood simulations have been carried out using the proposed combinations by Taguchi (L27 and L9 orthogonal arrays) to investigate the influence of four key input parameters, namely mesh size, runoff coefficient, roughness coefficient, and precipitation intensity. The results indicate that the methodology is adequate for sensitivity analysis, and that the precipitation intensity is the dominant parameter. Furthermore, the model calibration based on local variables (cross-sectional water level) can be inaccurate to simulate global variables (flooded area).

Key words: 2D hydrodynamic flood modeling, ANOVA, global sensitivity analysis, Taguchi design

HIGHLIGHTS

- A Taguchi–ANOVA approach can be used as an efficient sensitivity analysis method in 2D flood modeling.
- Necessity of considering both local- and global-scale calibrations is shown.
- The great importance of accurate estimation of precipitation intensity in flood simulation is presented.
- Mesh refinement sometimes can affect the results negatively.
- The significance of the input parameters can change depending on the hydrological conditions.

INTRODUCTION

In hydrologic modeling, the use of 2D hydrodynamic models is common in applications like floods or water quality assessment (e.g., Yu & Lane 2006; Park et al. 2014; Zischg et al. 2018). Those models, based on the numerical solution of the 2D shallow water equations (SWEs), use different types of input parameters with complex domain spaces (e.g., hydrological data, floodplain and channel geometry, initial and boundary conditions, and roughness). Most of these parameters cannot be measured directly and can only be inferred by calibration to observed system responses (Ghasemizade et al. 2017; Zadeh et al. 2017). As a result, input parameters are one of the main sources of uncertainty in flood simulation processes, and a considerable amount of literature has investigated the relative importance of the inputs of interest and their contributions to the numerical models' outputs.

In 1D simulations, particular attention has been given to input parameters such as hydraulic roughness coefficient in the river channel and flood plains (e.g., Pappenberger et al., 2005; Werner et al. 2005; Schumann et al., 2007; Papaioannou et al., 2017), discharge and design hydrograph (e.g., Ahmadisharaf et al. 2018; Chen et al. 2018; Vojtek et al. 2019). In 2D simulations, the analysis has been extended to other inputs such as topography/bathymetry and digital terrain model (DTM) resolution (e.g., Mejia & Reed 2011; Neal et al. 2015; van Vuren et al. 2015; Abily et al. 2016; Savage et al. 2016; Lim & Brandt 2019), mesh type, and mesh resolution (Schubert et al. 2008; Dottori et al. 2013; Zhang et al. 2016; Hu et al.

2019). Among the considered parameters, hydraulic roughness is usually considered the most influential and is, therefore, given first consideration in the model calibration (Teng *et al.* 2017).

In recent years, due to the advances in computational power of computers and accessibility of graphics processing units (GPU), hydrodynamic models are becoming increasingly complex which intend to apply inputs and processes similar to what happens in nature such as spatially/temporally varying precipitation, high spatial resolution data that represent more details and infiltration/drainage processes. One example is the study conducted by Sauer & Ortlepp (2021), in which different rainfall scenarios are defined (time and space invariant, space invariant and time varying, and space and time varying) over a small area (12 km²), and the relative influence of hydraulic roughness coefficients and DTM resolution on the models' output has been roughly assessed with a simple sensitivity analysis (SA). They concluded that rainfall data, as well as the spatial resolution of the digital elevation model, have a strong influence on the surface runoff dynamics in terms of water levels in space and time. The effect of different input parameters including spatial resolution, rainfall inputs, and the parameters which are linked with the land-use information such as roughness and drainage has been investigated in a hydrodynamic urban flood simulation by Xing *et al.* (2021) using a detailed SA for a very small catchment (0.59 km²). They reported that model sensitivity to the input parameters can vary depending on the outputs choice. They found that the influence of the spatial resolution is more tightly related to the flood flow movements, whereas that of the rainfall inputs is more relevant to the flood water volume.

Most of the hydrodynamic simulations in the above-mentioned studies were performed in small areas or limited specific river reaches. Few studies were made at a bigger catchment scale. Some examples are the study by Fernández-Pato *et al.* (2016) that investigated the influence of infiltration, and the studies by Bellos *et al.* (2020) and Zischg *et al.* (2018) that analyzed the effect of precipitation spatial patterns. According to the literature, still little attention has been paid to the influence of parameters such as infiltration, runoff coefficient, spatially/temporally varying precipitation, and the possible interaction between them.

Beside the importance of input parameters in the modeling process, one of the key preliminary steps for the application of the physically based distributed modeling based on the 2D SWEs is the generation of a computational mesh (Ferraro *et al.* 2020). In this context, many studies have investigated the effect of mesh structure, shape, and size on the accuracy of the simulated results and computation time (Caviedes-Voullième *et al.* 2012; Gibson *et al.* 2016; Hu *et al.* 2018). Some of the studies reported that there is no optimal mesh type for 2D flood modeling, because each element type (e.g., triangle and quadrilateral) is advantageous under different circumstances (e.g., Kim *et al.* 2014), while some tried to address ways to generate the most optimum computational mesh (acceptable degree of accuracy and computational costs) (e.g., Bomers *et al.* 2019; Ferraro *et al.* 2020). Most of these studies were performed in small scales such as flood plain scale or urban areas, while a few studies have assessed the issue at the catchment scale with regard to possible interactions between land-related features (i.e., friction, infiltration, and runoff coefficient) (e.g., Caviedes-Voullième *et al.* 2012; Costabile & Costanzo 2021).

The quest for developing accurate and computationally efficient simulations prompts the need for understanding the models' behavior under different conditions, which can be offered by SA methods.

SA methods can be broadly classified into local and global methods (van Griensven *et al.* 2006; Campolongo *et al.* 2011; Tian 2013; Song *et al.* 2015). Local sensitivity measures, often referred to as 'one at a time' measures, assess how variation in one input affects the model output keeping the other inputs fixed to a nominal value (Campolongo *et al.* 2011). The main drawback of local SA methods is that interactions among inputs cannot be detected (Campolongo *et al.* 2011), which can render nonreliable results for complex and nonlinear systems (Yang 2011), where input factors usually interact with each other. In contrast, global SA methods can be used as a reliable approach to investigate the influence of inputs on outputs while they are varied simultaneously over their entire domain space. Song *et al.* (2015) reviewed various types of global SA methods in the field of hydrological modeling and provided a framework for SAs in hydrological modeling. Pianosi *et al.* (2016) also provided a comprehensive review of existing SA methods following different end purposes such as uncertainty assessment, model calibration, diagnostic evaluation, dominant control analysis, and robust decision-making in a classified context. SA methods have been used in hydrodynamic modeling, mainly focusing on the uncertainties arising from model parameters and inputs.

Most of the studies mentioned above use global SA methods. The main drawback of the global SA methods is that they are computationally intensive, time-consuming, and require too many simulations. Therefore, global SA is often difficult to be applied in engineering practice and to overcome that the number of required simulations must be drastically reduced. In

that path, the methods and expertise accumulated in the field of design of experiments (DoE) (named after Rao 1947) can be useful for developing a time and cost-effective design for performing SA under various conditions.

The DoE is a statistical approach to reaction optimization that allows the variation of multiple factors simultaneously in order to screen 'reaction space' for a particular process (Murray *et al.* 2016). Making an analogy between experiments and simulations, the statistical DoE can be implemented as a method to effectively reduce the number of simulations (experiments) and explore the relationship between the input parameters (predictor variables) and the generated output (response variables), as well as various interactions that may exist between the input variables (Yuangyai & Nembhard 2010; Khang *et al.* 2017; Whitford *et al.* 2018). This approach can be classified as a global SA method since several parameters are varied systematically and simultaneously to obtain sufficient information (Whitford *et al.* 2018).

Taguchi (1986) has developed a methodology for the application of designed experiments based on orthogonal design to reduce the number of experimental combinations. A large number of studies about the successful application of the Taguchi method can be found in laboratory experimental practices, manufacturing, and design processes (e.g., Rao *et al.* 2004; Sadeghi *et al.* 2012; Hadi *et al.* 2017). But no previous study has used the Taguchi method in hydrodynamic flood simulations.

The present study presents a global SA of flood simulations solving the 2D SWE at the catchment scale (for a big catchment, 1,767 km^2), involving various parameters at different levels, in which each simulation takes a long time (about 3 h using 8× NVIDIA Tesla P100 (16 GB) GPU (Model: 2× Intel(R) Xeon(R) CPU E5-2698 v4@2.20 GHz)). Considering these features, the Taguchi method has been chosen. The main purpose of this paper is, therefore, to evaluate the application of the Taguchi method as a feasible engineering SA tool for 2D hydrodynamic simulations at the catchment scale and to identify the most influential parameters.

CASE STUDY

Tovdal river, located in Agder province (Norway), is selected as the case study. The computational domain is the part of the catchment upstream of the small lake named Flaksvann, just beside a town called Birkeland (Figure 1). In order to avoid the outlet boundary interference, the domain was extended 11 km further to the downstream of the lake. The length of the main river reaches approximately 130 km, and the catchment with an area of about 1,767 km^2 is dominated by forests (about 74%). The elevation ranges from 10.00 to 872.34 m.a.s.l, and the average slope of the catchment along the river is about 0.65%. The mean annual precipitation is approximately 1,261 mm, with most of the rainfall occurring between October and March (about 60%). On 2 October 2017, an extreme flood event occurred in this area which was the highest ever recorded flood in this river. Recorded data of the event (Table 1) (including recorded water level, discharge, flood hydrograph at Flakksvann cross-section (CS), and flood maps) and a 2D hydrodynamic model were used to simulate the event and validate the methodology. For the calibration process, the weighted average of precipitation intensities which occurred 1.5 days before the 2017 flood event was used as the reference precipitation (Table 1). Subsequently, by adjusting the friction factor and the runoff coefficient values for each land class in a trial-and-error process, calibration was performed such that simulated water level and discharge resembled the event's recorded information (Table 1).

METHODS

Hydrodynamic model

In the current study, a GPU-based 2D horizontal hydrodynamic model named HiSTAV was used to simulate floods. The model was originally proposed by Ferreira *et al.* (2009) and optimized by Conde *et al.* (2020). The core of the model is a hyperbolic system of partial differential equations expressing mass and momentum conservation principles for flow. The model is closed in terms of flow resistance and a specific return-to-capacity parameter by a modified closure model. The SWEs are solved using a finite volume scheme, which is applied on a spatial discretization using unstructured meshes. The discretization method allows body fitting unstructured grids which can optimize the computational workload by using large cells, where flow gradients are expected to be mild and small cells in specified areas. The detailed information about HiSTAV and the model structure can be found in the study presented by Conde *et al.* (2020).

Simulation set-up and approach

In order to simulate the flow, the model solves the equations based on the following sources:
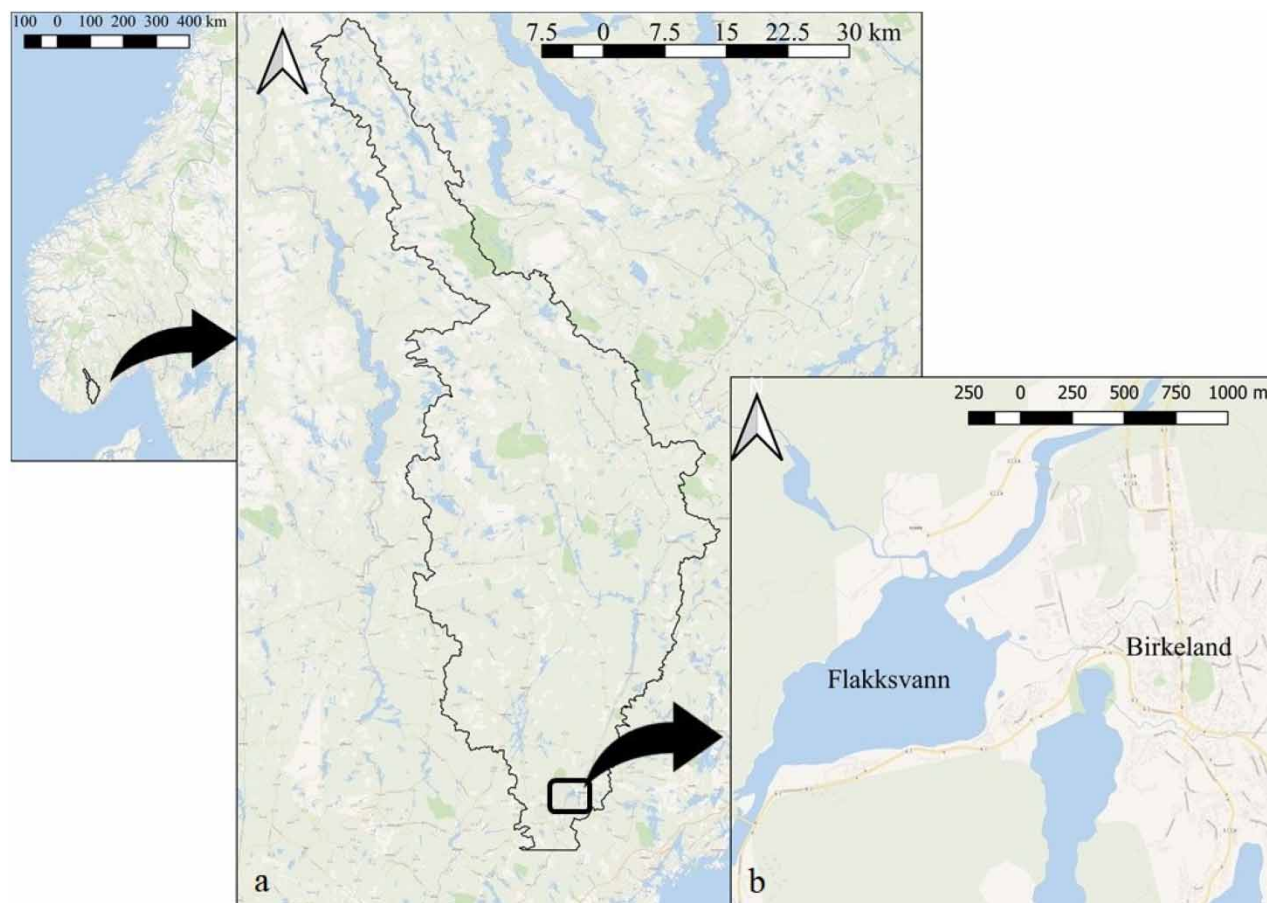
Figure 1 | (a) Map of the Tovdal river catchment area until the computational domain and (b) the flooded area (Birkeland town area).

Table 1 | The recorded data of the flood event in the study area (water level and discharge refer to Flakksvann, in Figure 1)

Date	Precipitation (mm)	Maximum water level (m)	Maximum discharge (m³/s)
30.09.2017	45.1	21.40	501.28
01.10.2017	173.1	24.57	1,061.19
02.10.2017	63.6	25.56	1,194.88

1. Input variables
2. Computational mesh
3. Initial and boundary conditions

The 2D model used here requires different data sets drawn from two main sources: (a) raster data structures including the topo-bathymetric dataset, Strickler roughness coefficient values, and runoff coefficient values, and (b) precipitation records including the spatial distribution of rainfall measurement stations.

Raster data structures and grids are used to present the catchment discretization and to describe spatially distributed terrain parameters (i.e., elevation, bathymetry, land use, etc.). A $10 \times 10 \ m^2$ DTM including the river bathymetry information is used to represent topographic features and derive hydrologic characteristics (i.e., slope, flow direction, flow accumulation, stream network, computational cascade for flow routing, etc.).

Hydraulic roughness is inserted in the model in the form of a grid structure raster file ($100 \times 100 \ m^2$ resolution), in which each cell represents Strickler roughness values. The spatial distribution of roughness values is determined based on $100 \times 100 \ m^2$ land cover maps (obtained from https://land.copernicus.eu/- 'Corine Land Cover 2018, Version 20').

Subsequently, using typical Strickler roughness coefficient tables, the roughness values were assigned for each cell (Arcement & Schneider 1989; Dorn et al. 2014). Different land types are classified in Table 2, and possible roughness variation ranges are assigned for each class.

The runoff coefficient C is a dimensionless factor that is used by HiSTAV to convert the rainfall amounts to runoff (effective precipitation $h_p = C \cdot i_P$ in Equation (1), being i_P the precipitation intensity). In this study, we used the runoff coefficient as a parameter which reflects the lumped effect of several processes such as the antecedent conditions of the catchment and infiltration, land cover effect, and spatial variability of the rainfall intensity. The concept of event runoff coefficients is widely used in hydrologic modeling (e.g., Merz et al. 2006; Merz & Blöschl, 2009; Viglione et al. 2009; Chen et al. 2019). The choice of runoff coefficient values was based on the average antecedent conditions for the catchment and land features. The values were then calibrated in a way that the correspondence of the event's rainfall and 2017 flood flow (level and velocity) is achieved. Similar to the hydraulic roughness values, the runoff coefficient is used in the form of raster data.

In this study, a combination of two different approaches to calculate the runoff coefficient was used. Firstly, by using land cover maps and recommended values of runoff coefficient for different types of areas (Subramanya 2013), a range was determined for each cell. Secondly, since the HiSTAV model assumes a uniform spatial distribution of precipitation as input, the runoff coefficient was used as an artifact to introduce spatial variability of the precipitation. For this purpose, focusing on the flood of 2 October 2017, daily precipitation data were obtained from 37 stations (Figure 2). The rainfall observations at the stations were interpolated to delineate the spatial distribution of precipitation. For this purpose, the inverse distance weighting interpolation method was used, giving similar precipitation patterns like the one presented by the Norwegian Meteorologic Institute (http://www.senorge.no/). Thereafter, precipitation zones were delineated in Figure 2. The combination of the two mentioned approaches was used to calculate the final runoff coefficient in each cell, C, as follows:

$$C = C_{initial} \times \left(\frac{i_{P_{cell}}}{i_{P_{max}}} \right) \tag{1}$$

where $i_{P \max}$ is the maximum amount of precipitation intensity among the recorded values, $i_{P_{cell}}$ is the recorded precipitation intensity in each cell, and $C_{initial}$ is the runoff coefficient with values displayed in Table 2 for each land cover class.

In order to define a reliable and time-consistent range to consider different flood magnitudes, three different rainfall intensities, i_P ranging from 3 to 9 mm/h, with a duration equal to 2 days, were considered for the simulations (Table 3). The range is obtained based on the average precipitation intensity that occurred in the flood event (6 mm/h) with 50% bounds. This means that the precipitation is treated as time invariant (or as block), which is rather a coarse and simplistic approach to the real conditions. Nevertheless, since the main goal of this study is to check the feasibility of using a simplified method (Taguchi method) for performing a global SA, we focus on reducing to a minimum number of inputs while having input ranges that cover in the full input–output space. This was needed because for such a big catchment, the inclusion of more inputs (like synthetic hyetographs defined by several parameters) would render many simulations.

HiSTAV employs adaptable triangular meshes in order to discretize the catchment and balance acceptable computational workloads, different detail levels, and complex geometry fitting capabilities (Conde et al. 2015). In this study, by employing

Table 2 | The land-use classes and corresponding ranges for the Strickler roughness coefficient and runoff coefficient

Land-use class	Occupied area (%)	Strickler roughness (K_s, m$^{1/3}$/s)	Runoff coefficient (C, %)
Constructed lands (discontinuous urban fabric, industrial, or commercial units)	0.40	40–70	80–90
Forests (broad-leaved, coniferous)	73.75	15–40	50–70
Moors and heathland	8.23	18–35	60–80
Agriculture and vegetated areas	12.82	18–37	40–60
Water courses and water bodies	4.76	20–50	100–100
Mineral extraction sites	0.04	30–60	70–90

Note: The median values of the specified ranges correspond to the calibrated values.
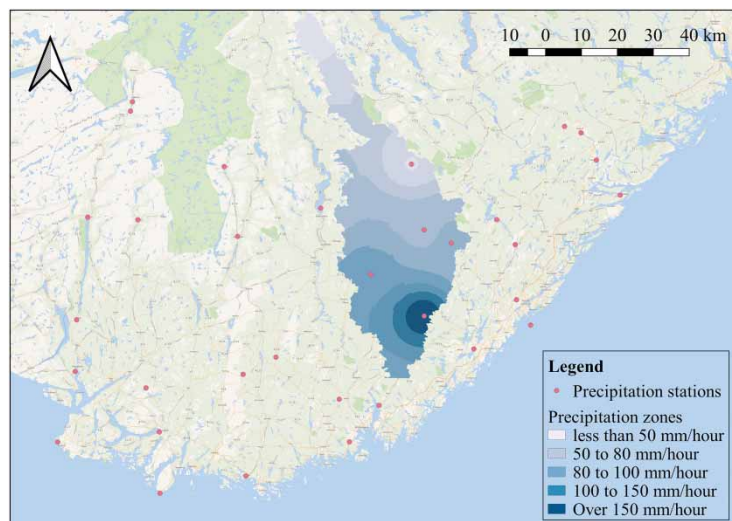
Figure 2 | Spatial distribution of the precipitation stations and the interpolated precipitation over the catchment.

Table 3 | Input parameters considered for the sensitivity analysis and their ranges of variation

Parameters		Level 1	Level 2	Level 3
Mesh size (m)	Maximum mesh length in the river (main channel)	15	20	25
	Maximum mesh in the flood plain	150	200	250
Precipitation intensity (mm/h)		3	6	9
Strickler roughness ($m^{1/3}$/s)	Constructed lands (discontinuous urban fabric, industrial, or commercial units)	40	50	70
	Forests (broad-leaved, coniferous)	15	25	40
	Moors and heathland	18	24	30
	Agriculture and vegetated areas	18	28	37
	Water courses and water bodies	20	35	50
	Mineral sites	30	40	60
Runoff coefficient (%)	Constructed lands (discontinuous urban fabric, industrial, or commercial units)	80	85	90
	Forests (broad-leaved, coniferous)	50	60	70
	Moors and heathland	60	70	80
	Agriculture and vegetated areas	40	50	60
	Water courses and water bodies	100	100	100
	Mineral sites	70	80	90

Note: The levels 1, 2, and 3 for mesh size are representative of the fine resolution (total number of mesh elements: 582,161), the medium resolution (total number of mesh elements: 473,265), and the coarser resolution (total number of mesh elements: 401,769), respectively.

Godunov's finite volume approach (LeVeque 2002), a mixed mesh of triangular cells are constructed in three sizes over the computational domain by Gmsh (Geuzaine & Remacle 2009), which is a free finite element grid generator with a built-in CAD engine and post-processor. The small cells or so-called finer resolutions are assigned to the cells where the flow gradients are expected to be large such as the river channel, medium-sized cells, or average resolution over the flood plain, and coarser resolution over other parts of the catchment, where flow gradients are expected to be mild (Figure 3). In the post-processing step, the constructed meshes were checked for shape and size quality. The initial conditions for the equations are zero water depth and zero discharge everywhere (dry surface conditions). Water enters the domain only through rainfall; hence there are no inlet boundaries. The only open boundary is at the outlet (downstream), where free outflow is assumed. Warm-up simulations were performed until reaching the normal water level in the river network. A 9-day precipitation with an intensity of 2 mm/h was found to be long enough to fill the river basin and the lakes with the steady flow over the main water courses.
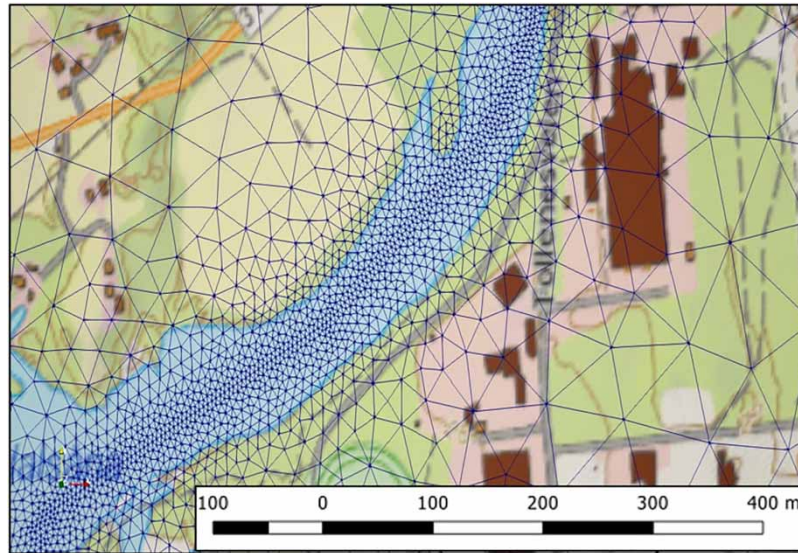
Figure 3 | Finite volume meshes at three different sizes.

Taguchi method

Taguchi developed a system of tabulated designs (arrays) that allows for the maximum number of main effects to be estimated in an unbiased manner while using only a minimum number of experimental tests (Taguchi 1986). He introduced his approach using experimental design aiming to develop a process to be robust to component variation and also to minimize variation around a target value (Ross & Ross 1988).

The process of Taguchi analysis can be summarized into seven steps (Bao *et al.* 2013). The flow chart of the whole process is illustrated in Figure 4.

In this study, the local water level and total flooded area are selected as objective parameters. To calculate these parameters, nine different CS are specified in Figure 5. Several different CS were chosen to cover the changes in hydrodynamic behavior of the river, and the water level is observed at the time step equal to 34 h (this time step is selected based on the duration of the 2017 flood event). The CS were selected at different locations such as the areas of key importance, adjacent to bridge structures, adjacent to the flow measure stations (level and velocity), and at locations that represent different geometries of the river. Therefore, two of the CS were chosen on the lake where the geometry and flow conditions differ from other parts of the river to assess the flow behavior and water-level sensitivity.

The total flooded area was delineated as the subarea starting from the Birkeland city region and extended to the end of the computational domain, which represents around 11 km along the main river.

The most important stage in the design of an experiment is the selection of the control factors. In this study, we selected the following four control factors: mesh size, hydraulic roughness parameter (K_S), runoff coefficient (C), and precipitation
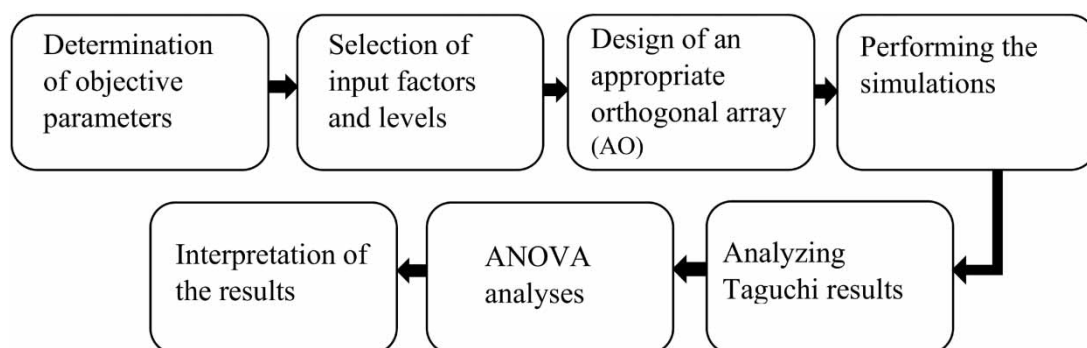

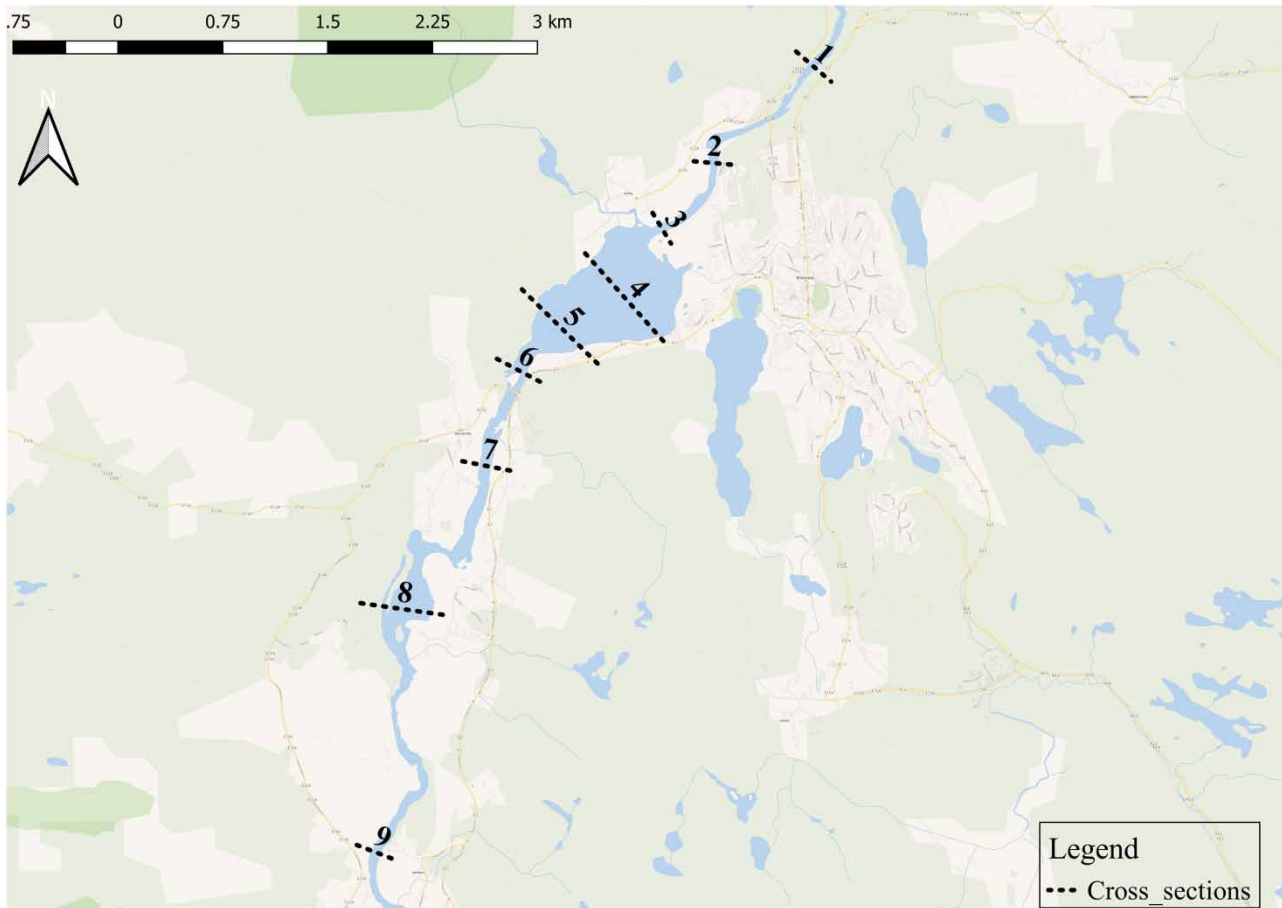**Figure 4** | The general framework of Taguchi–ANOVA analyses.

Figure 5 | Cross-sections' locations.

intensity (i_P). These factors reflect the set of data, in which HiSTAV uses as an input to simulate the flow. We assigned three values to each of these control factors, as shown in Table 3. The three levels reflect the possible variation range for each parameter.

In the full factorial design, all possible combinations for a given set of factors are considered (Fanchi 2005), which, depending on the number of factors and associated levels, can result in a large number of experiments. The Taguchi method uses the orthogonal design to reduce the number of combinations. Using orthogonal arrays allows us to collect the necessary information by testing specific combinations, instead of examining all possible combinations. The orthogonal arrays have special properties such as (i) all the levels appear an equal number of times (balancing property), (ii) all the levels of parameters (factors) are used for conducting the experiments, and (iii) the array of each factor columns is mutually orthogonal to any other column (Kacker *et al.* 1991). Accordingly, the sequence of levels for conducting the experiments follows a standard sequence and cannot be changed. There are many standard orthogonal arrays available, depending on the number of parameters and the levels of variation for each parameter. Detailed information on the construction of orthogonal arrays can be found in the works presented by Plackett & Burman (1946) and Taguchi (1986).

The full combination of the experiments (full factorial design), considering four parameters with three levels, corresponds to 81 simulations. However, to effectively reduce the number of experiments, the Taguchi method proposes two possible orthogonal arrays, namely L27 and L9. The L27 consists of 27 sets of combinations and assesses the main effects and the interaction between the parameters, while the L9 consists of nine combinations, which only concentrates on main effects and ignores the interactions.

According to the importance of the interactions between the parameters in SA studies, this study is mainly focused on the L27 array. However, the results for the L9 array are also briefly presented to identify the possibility of performing the SAs with the minimum number of experiments. To validate the performance of the implemented method, the results were benchmarked against the results obtained from all the possible combinations of simulations (L81).

Table 4 | L9 design and calculated SNR values for the water level at nine CS (CS1–CS9) and total flooded area

| No. | Levels | | | | SNR | | | | | | | | | |
	Mesh	c	K_S	i_P	CS1	CS2	CS3	CS4	CS5	CS6	CS7	CS8	CS9	Area
1	1	1	1	1	30.674	26.598	26.505	26.502	26.502	26.495	26.372	26.248	25.089	6.833
2	1	2	2	2	31.016	27.283	27.213	27.213	27.213	27.197	27.071	26.913	25.828	8.331
3	1	3	3	3	31.536	28.353	28.343	28.343	28.343	28.307	28.167	27.907	26.866	10.385
4	2	1	2	3	31.072	27.390	27.330	27.330	27.330	27.312	27.180	27.022	25.869	8.606
5	2	2	3	1	30.613	26.358	26.292	26.293	26.293	26.285	26.201	26.136	24.926	6.419
6	2	3	1	2	31.167	27.748	27.679	27.677	27.676	27.661	27.488	27.271	26.101	9.136
7	3	1	3	2	30.844	26.764	26.707	26.707	26.707	26.697	26.607	26.491	25.319	7.312
8	3	2	1	3	31.378	28.222	28.171	28.169	28.168	28.148	27.967	27.711	26.535	9.931
9	3	3	2	1	30.758	26.632	26.563	26.562	26.562	26.554	26.452	26.342	25.167	6.943
Mean					31.006	27.261	27.200	27.199	27.199	27.184	27.056	26.893	25.744	8.211
Standard deviation					0.299	0.689	0.703	0.703	0.703	0.695	0.669	0.607	0.637	1.343
Coefficient of variation					0.010	0.025	0.026	0.026	0.026	0.026	0.025	0.023	0.025	0.164

The L9 and L27 orthogonal arrays (see first five columns in Tables 4 and 5) were constructed using the aforementioned factors (Table 3) based on the Taguchi method (Kacker *et al.* 1991). Following the combinations constructed in the orthogonal tables, the simulations were then performed, and the identified objective outputs were calculated as the system's response.

The Taguchi design uses the signal-to-noise ratio (SNR) to measure the deviation of the response from the mean value (Wang *et al.* 2017). Based on the purpose of the experiment, SNRs can be classified into three types: smaller the better type (minimize the response), larger the better type (maximize the response), and nominal the best type (based on the SNR on standard deviation). The equation to calculate SNR values for larger the better type is presented in the following equation:

$$SNR = -10 \times \log\left(\frac{1}{n}\sum_{i=1}^{n}\frac{1}{Y_i^2}\right) \tag{2}$$

where Y_i represents the measured results in the ith experiment/simulation and n is the number of experiments/simulations.

.To investigate the conditions that result in the major flood, the goal is defined as larger the better. Therefore, the larger values for the water level and the flooded area are desirable, and the SNR is calculated by Equation (2). The averages of the SNR values are calculated for each factor j at level l using the following equation to analyze the effect of each factor on the outputs:

$$MSNR_{Factor=j}^{Level=l} = \frac{1}{n_{jl}}\sum_{i=1}^{n_{lj}}[SNR_{Factor=j}^{Level=l}]_i \tag{3}$$

where n_{jl} is the number of experiments that have factor j at level l and i represents the ith experiment with factor j at level l. The significant parameters were then identified as those producing the highest difference in the mean SNR and mean response (target outputs) values. To find the rank of the effect of each parameter in the Taguchi analysis results, a parameter (Δ_j) is defined, which is the difference between the maximum and minimum SNR of all levels for each factor (see Figure 8 and the example in Figure 6(a)). Higher values for (Δ_j) indicate that the model has a higher sensitivity to factor j.

Analysis of variance

In addition to the SNR analysis, analysis of variance (ANOVA) was performed to identify the most significant factors and their potential interactions. This method focuses on the analysis of the variance explained by each factor and is accomplished by estimating Fischer's test value (F-value). The impact of any factor is explained by its F-value and the corresponding sum of squares that represent variance. Higher F-value and sum of squares of any factor indicate its relative importance in the

Table 5 | L27 design and calculated SNR values for the water level at nine CS (CS1–CS9) and total flooded area

	Levels				SNR									
No.	Mesh	c	K_S	i_P	CS1	CS2	CS3	CS4	CS5	CS6	CS7	CS8	CS9	Area
1	1	1	1	1	30.674	26.598	26.505	26.502	26.502	26.495	26.372	26.248	25.089	6.833
2	1	1	2	2	30.892	27.014	26.930	26.929	26.929	26.915	26.801	26.666	25.554	7.743
3	1	1	3	3	31.123	27.438	27.397	27.398	27.398	27.378	27.263	27.105	26.020	8.720
4	2	2	1	1	30.738	26.787	26.704	26.701	26.701	26.693	26.563	26.431	25.235	7.313
5	2	2	2	2	30.935	27.096	27.026	27.026	27.026	27.011	26.892	26.764	25.582	7.976
6	2	2	3	3	31.259	27.692	27.660	27.661	27.661	27.636	27.513	27.348	26.227	9.131
7	3	3	1	1	30.834	26.948	26.868	26.865	26.865	26.857	26.727	26.569	25.375	7.590
8	3	3	2	2	31.140	27.503	27.453	27.452	27.452	27.437	27.313	27.094	25.952	8.795
9	3	3	3	3	31.494	28.182	28.167	28.166	28.166	28.140	28.004	27.763	26.713	9.987
10	2	3	1	2	31.167	27.748	27.679	27.677	27.676	27.661	27.488	27.271	26.101	9.136
11	2	3	2	3	31.460	28.219	28.187	28.186	28.185	28.160	27.987	27.756	26.666	10.045
12	2	3	3	1	30.660	26.468	26.404	26.405	26.405	26.397	26.310	26.239	25.026	6.720
13	3	1	1	2	30.949	27.234	27.162	27.160	27.160	27.150	27.012	26.825	25.632	8.236
14	3	1	2	3	31.110	27.461	27.411	27.410	27.410	27.395	27.276	27.060	25.919	8.734
15	3	1	3	1	30.635	26.265	26.212	26.210	26.210	26.203	26.121	26.054	24.820	5.853
16	1	2	1	2	31.087	27.663	27.596	27.594	27.594	27.577	27.419	27.202	26.048	9.007
17	1	2	2	3	31.348	28.102	28.071	28.070	28.070	28.041	27.889	27.647	26.578	9.872
18	1	2	3	1	30.642	26.398	26.313	26.314	26.314	26.303	26.224	26.143	24.988	6.423
19	3	2	1	3	31.378	28.222	28.171	28.169	28.168	28.148	27.967	27.711	26.535	9.931
20	3	2	2	1	30.705	26.512	26.444	26.444	26.444	26.436	26.336	26.235	25.044	6.632
21	3	2	3	2	31.004	27.084	27.031	27.033	27.033	27.017	26.924	26.771	25.598	7.874
22	1	3	1	3	31.714	29.060	29.032	29.031	29.030	29.000	28.799	28.478	27.252	11.383
23	1	3	2	1	30.786	26.744	26.649	26.648	26.648	26.637	26.529	26.417	25.292	7.153
24	1	3	3	2	31.209	27.573	27.533	27.535	27.535	27.513	27.398	27.224	26.151	8.909
25	2	1	1	3	31.146	27.742	27.678	27.676	27.675	27.660	27.489	27.274	26.106	9.156
26	2	1	2	1	30.603	26.352	26.280	26.279	26.279	26.272	26.172	26.095	24.895	6.246
27	2	1	3	2	30.782	26.713	26.650	26.651	26.651	26.641	26.547	26.464	25.248	7.200
Mean					31.011	27.280	27.221	27.220	27.220	27.203	27.078	26.912	25.756	8.244
Standard deviation					0.293	0.676	0.690	0.690	0.690	0.683	0.657	0.597	0.623	1.358
Coefficient of variation					0.009	0.025	0.025	0.025	0.025	0.025	0.024	0.022	0.024	0.165

process of the response (Karmakar *et al.* 2018). Moreover, to explore the impacts of individual factors, the percentage contribution (*PC*) of each factor is calculated using the following equation (Yang & Tarng 1998; Sadrzadeh & Mohammadi 2008):

$$PC = \frac{SS_j}{SS_T} \times 100 \tag{4}$$

where SS_T is the total sum of squares and SS_j is the sum of squared deviations for each factor j. Both can be calculated using
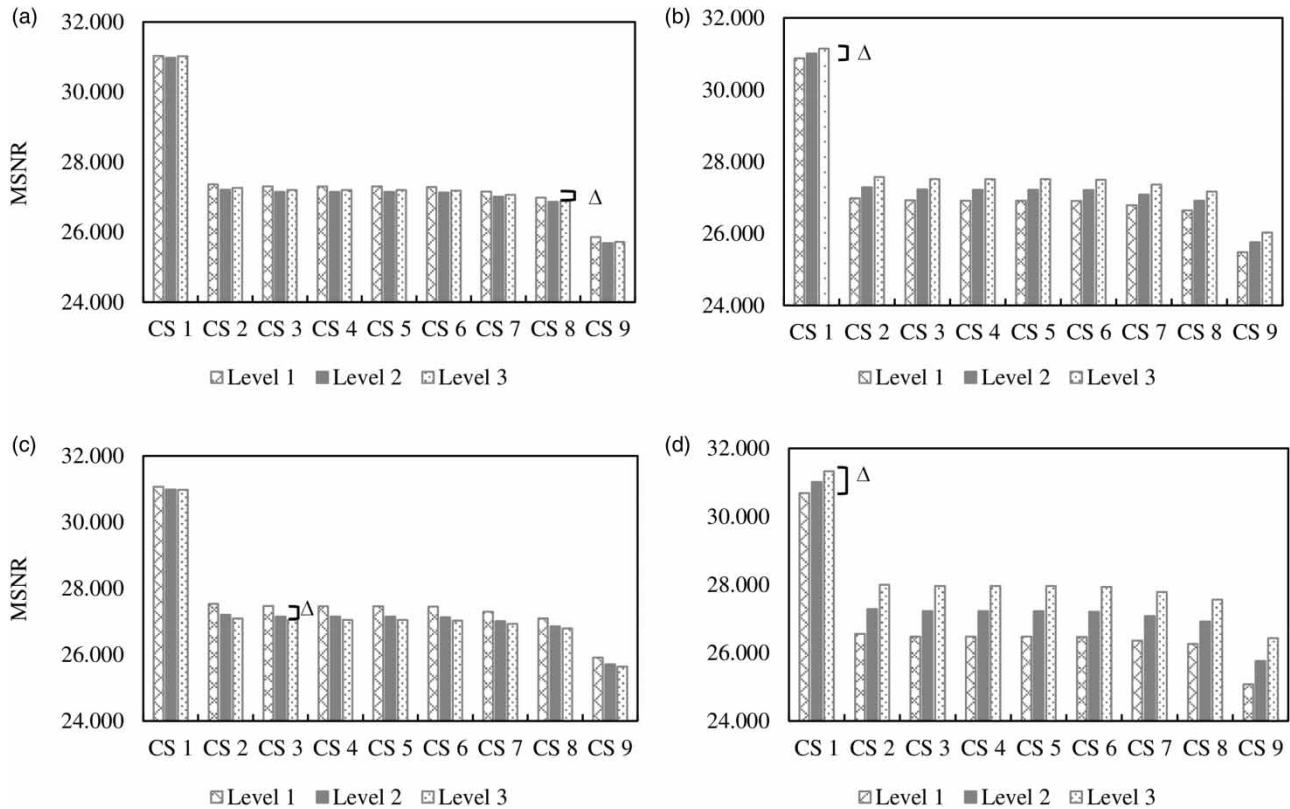
Figure 6 | Calculated mean SNR at each level for (a) mesh parameter, (b) runoff coefficient, (c) roughness coefficient, and (d) precipitation intensity (considering the cross-sectional water level as a system response).

the following equations, respectively:

$$SS_T = \sum_{i=1}^{n} (Y_i - \bar{Y})^2 \tag{5}$$

$$SS_j = n_{jl} \sum_{i=1}^{l} (\overline{Y_{ji}} - \bar{Y})^2 \tag{6}$$

where n is the number of experiments/simulations, Y_i represents the measured results in the ith experiment/simulation, $\bar{Y}$ is the average of results, $\overline{Y_{ji}}$ is the mean of results for the factor j at level i, and n_{jl} is the number of experiments that have factor j at level l (Stahle & Wold 1989).

RESULTS AND DISCUSSION

Following the combinations constructed in the Taguchi tables (Tables 4 and 5), 9 and 27 sets of simulations were performed. Two different output parameters, namely local water level and total flooded area, were considered as the system response to investigate the variation resulting from each combination and subsequently to explore the significance of each input parameter in the simulations. The calculated SNR values (based on Equation (2)) for the water level in each CS and the flooded area are presented in Tables 4 and 5.

The calculated standard deviation for the SNR values in each of the local responses (CS water level) ranges between 0.29 and 0.69 for L27 (see Table 5) and for the global response (flooded area) it is equal to 1.36. The coefficient of variation which is defined as the ratio of the standard deviation to the mean is calculated to measure the degree of variation in each of the results series (Tables 4 and 5). The higher coefficient of variation values for the flooded area indicates that it is much more sensitive than the local water level. This result is important because in most of the applications, the hydrodynamic models are
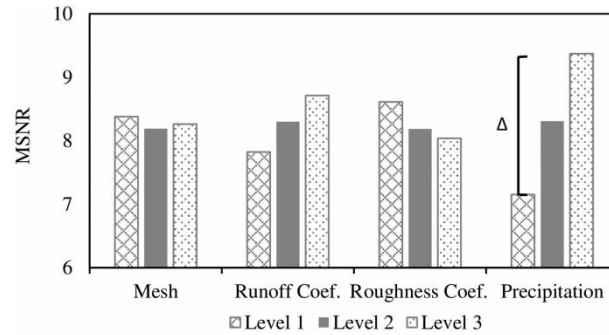
Figure 7 | Calculated mean SNR for each parameter (considering the flooded area as a system response).

calibrated based on local variables (e.g., water level) with some known inputs (e.g., precipitation intensity) and some particular combinations of calibrated inputs (e.g., runoff coefficient, roughness coefficient, and mesh), which after all can correspond to a quite different flooded area if a different combination of calibrated inputs was used.

From Table 5, it can be seen that the highest SNR results from the combination 22 (1 3 1 3) for the water level and the flooded area, corresponding to the fine mesh size, highest runoff coefficient, smallest roughness coefficient, and highest precipitation intensity. This result is not surprising since the SNR is being computed with larger the better, i.e., the highest water level or the flood area will give the highest SNR.

In order to quantify the significance of each parameter, the mean of the SNR for each factor at the ith level was calculated using Equation (3) and is presented in Figures 6 and 7.

The results are compared and ranked based on Δ parameter for the L9, the L27, and the full factorial design (L81) in Figure 8. Moreover, the *PC* of each factor obtained from ANOVA is presented for the mentioned designs in Figure 9 (further details of the Taguchi and ANOVA analyses results are presented in the Supplementary Material).

As it is shown in Figures 8 and 9, for both responses (water level (panel a) and flooded area (panel b)) in all types of the designs, the precipitation intensity is the most influencing parameter, followed by the runoff coefficient, the roughness coefficient, and lastly the mesh. The only exception can be seen for CS1 and CS9 in L9 design, in which the mesh size and the
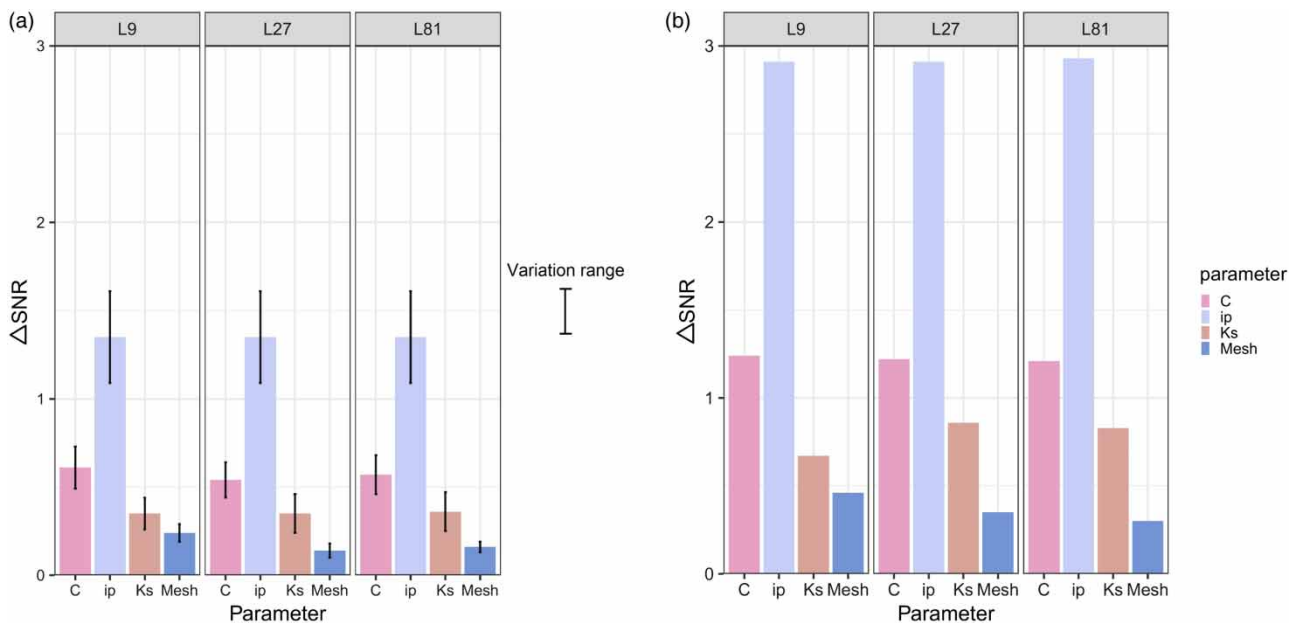

Figure 8 | Overview of ΔSNR variation for (a) local responses (the variation range shows the variation of ΔSNR values at different CS) and (b) global response.
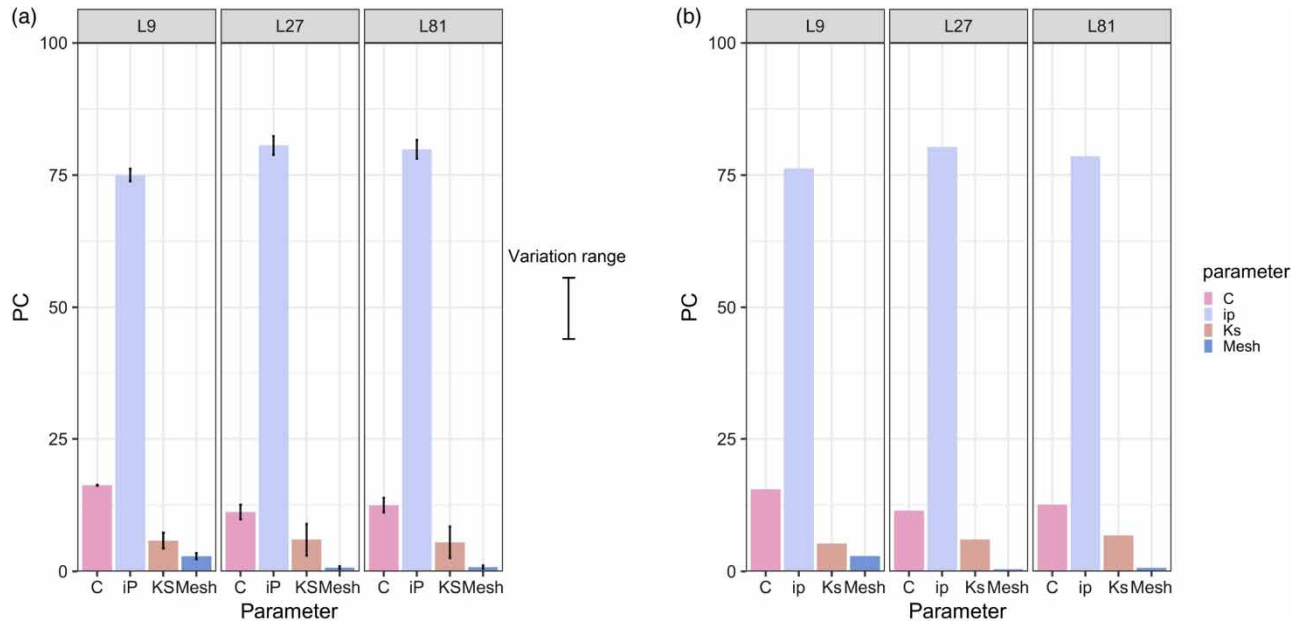
Figure 9 | Overview of the ANOVA analysis results for (a) local responses (the variation range shows the variation of *PC* values at different CS) and (b) global response.

roughness effect have equal ΔSNR values (0.12 and 0.3, respectively) and as a result are equally ranked as 3. However, comparing the L27 design results with the full factorial design (L81), it can be seen that there are no big differences between the results which means the results of the ANOVA and the Taguchi analyses using L27 combinations are consistent with those obtained from the full factorial design (L81). This finding confirms the effectiveness of the L27 design. Although the L9 design requires few numbers of experiments and provides results almost in accordance with full factorial design results, caution must be applied, as the findings in two of the CS (CS1 and CS9) showed that the mesh size effect has been overestimated by L9.

The results obtained from Figure 9 indicate that precipitation intensity is by far the most important factor, contributing about 80%, while the runoff coefficient and roughness coefficient contribute about 11 and 6%, respectively, and mesh accounts only for 1% contribution. This result highlights the huge importance of either estimating the precipitation intensity adequately with a given return period (which possibly has a big uncertainty due to climate change) for flood mapping or of predicting accurately the precipitation intensity (which has the uncertainty associated with the stochastic nature of weather) for flood forecasting systems. Also interesting is the fact that the runoff coefficient is slightly more relevant than the roughness coefficient. Usually, hydrology modelers attribute more relevance to the runoff coefficient, whereas hydraulic modelers focus on the importance of the roughness coefficient. From the joint hydrologic and hydraulic modeling, it seems that the runoff coefficient is quite relevant, which gives an indication to hydraulic modelers that the input discharge (usually coming from hydrological modeling, involving precipitation and runoff coefficient) influences their final results much more than the roughness coefficient.

The results in Figures 6 and 7 show that finer meshes (level 1) lead to slightly larger SNR values than coarser ones (levels 2 and 3). Nevertheless, the performance improvement with mesh refinement is not always true since the SNR value for the coarser mesh (level 3) is higher than the intermediate one (level 2). This puts in evidence that refining unstructured meshes with underlying complex topography can lead to no improvement. As stated before, for the runoff coefficient, roughness coefficient, and precipitation intensity, the performance results follow what is usually expected, i.e., the increase in runoff coefficient (levels 1–3) increases the SNR values, the increase in the Strickler coefficient (i.e., decrease in roughness, levels 1–3) reduces the SNR values and the increase in the precipitation intensity (levels 1–3) results in higher SNR values. This is confirmed by the maximum and minimum flooded areas, corresponding to combinations 22 and 15, respectively, that are presented in Figure 10.

In complex and nonlinear systems, the joint effects of input parameters can have a significant influence on the outputs. Thus, in order to have a complete SA, the interactions among parameters are analyzed using the ANOVA technique. In this regard,
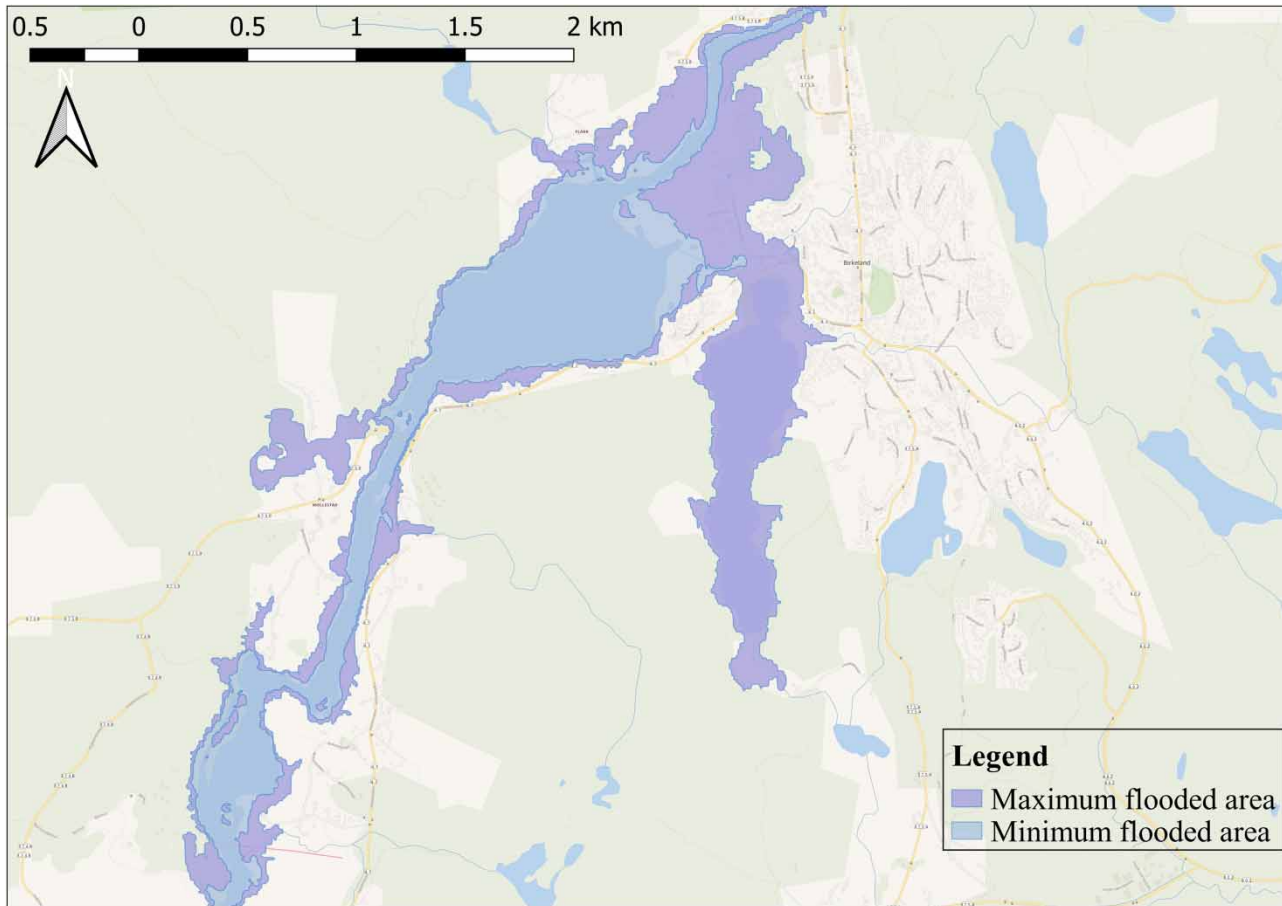
Figure 10 | The variation in the calculated flooded area.

CS4, which is considered an important CS located in the Flaksvann lake where a hydrological station exists, was selected to explore the interaction between the parameters. The interactions are analyzed for both L27 and L81 at a specified CS. Since the results were similar, the interaction matrix of the parameters is only presented for the L27 design in Figure 11. If the curves are parallel with each other, it means that there are no interaction effects of the two parameters (Wang *et al.* 2017).

The intersection lines in Figure 11(b) imply that the mesh size mostly interacts with the roughness coefficient, presenting similar performances for the rougher case (smaller Strickler coefficient, i.e., level 1), but a much more mixed behavior for less rough cases (levels 2 and 3). As can be seen in Figure 11(a)–11(c), and already mentioned, mesh refinement will not necessarily improve performance (i.e., the SNR). In Figure 11(b), the mesh refinement always improves the performance for the smoother case (roughness at level 3), but that is not true for the intermediate case (level 2), where a mesh refinement from level 3 to level 2 produces worse results. As stated before, this is related to the unstructured mesh generation, in particular, near the river main channel where the roughness coefficient varies. From those figures, it is seen that, in general, the intermediate mesh (level 2) presents lower performance, and the finer mesh (level 1) presents slightly better results than the coarser mesh (level 3). The latter becomes more evident for high-intensity precipitation (see level 3 in Figure 11(c)), which indicates that for simulating extreme flood events refining the mesh can originate a better performance.

The runoff coefficient slightly interacts with the precipitation intensity (Figure 11(e)). It is clear that runoff coefficients are more important for model performance as the intensity precipitation level is higher. This is logic since the runoff coefficient represents a precipitation percentage loss, which, for the same level (i.e., percentage) and higher intensity of precipitation, corresponds to a much higher amount of water flowing through the catchment (i.e., higher SNR). Nevertheless, this points out to the importance of a correct calibration of the runoff coefficient, especially for high-intensity precipitation events that originate floods.

Based on the mean response variation range (see blue dashed circles in Figures 11(e) and 11(f)), it can be observed that the importance of the parameters changes depending on the precipitation intensity. At the lower intensity (level 1), the roughness
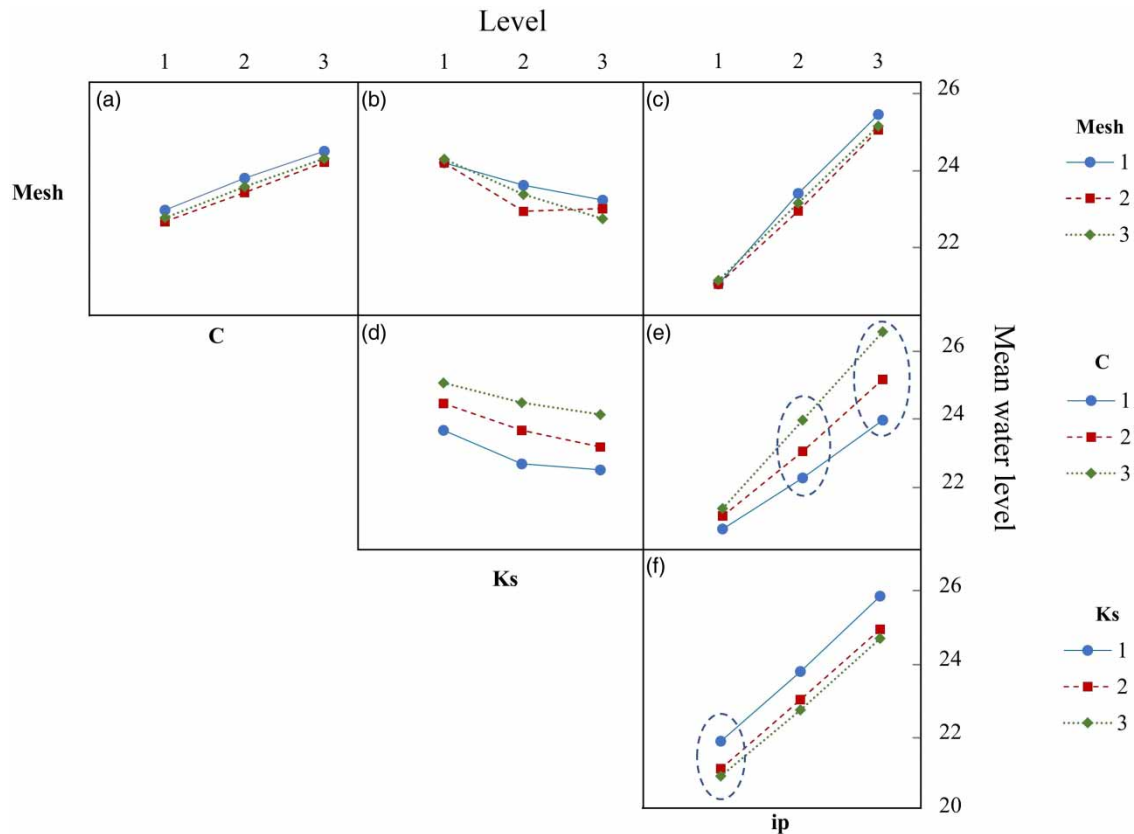
Figure 11 | Interaction plots for the water level at CS4. C is the runoff coefficient, K_S is the roughness coefficient, and i_p is the precipitation intensity. Interactions between: (a) mesh and C, (b) mesh and K_S, (c) mesh and i_p, (d) C and K_S, (e) C and i_p, and (f) K_S and i_p.

parameter corresponds to higher variation comparing to the other parameters. Whereas, under moderate and high intensities (levels 2 and 3), the runoff coefficient is the most influencing parameter, which corresponds to the higher variation range in the mean water level.

CONCLUSION

In this study, the application of the Taguchi technique and ANOVA was investigated to identify and rank the most influencing parameters in a 2D hydrodynamic flood simulation model. In general, this approach has several advantages: (i) it can effectively reduce the number of simulations needed for SA, (ii) it quantifies the contribution of each parameter and ranks them based on the associated variation in target outputs, and (iii) it explores the interaction between input parameters.

- The main conclusions of this study are: the implemented Taguchi–ANOVA approach can be used as an efficient SA method in 2D flood modeling to quantify and rank the affecting parameters. However, the results suggest that the minimum orthogonal array (L9) should be used cautiously and that an intermediate orthogonal array (L27) is preferred, if affordable.
- The considered global response (flooded area) is more sensitive to the input parameters variation comparing to the local response (cross-sectional water level). This shows the necessity of considering both local and global scale calibrations for flood simulation purposes.

The following secondary conclusions, which require further validation for a more complex hydrological approach, can be drawn from the results presented in this paper:

- The precipitation intensity is identified as the most significant parameter in flood modeling, accounting for about 80% contribution. Then follows runoff coefficients (11%), roughness coefficient (6%), and mesh size (1%). This highlights the great importance of accurate estimation of the precipitation intensity for flood modelers and decision makers. This can be a major challenge due to the uncertainties resulting from climate change and the stochastic nature of the weather.

- Generally, among the proposed mesh sizes, the finer mesh size (level 1) led to slightly better results compared with the other mesh sizes (levels 2 and 3). Especially, under high-intensity precipitation (level 3), the difference is clearer. However, the mesh refinement is not always a solution to improve the results due to the underlying complex gridded data, including topography, roughness, and runoff coefficient values. Moreover, the strong interaction between the roughness coefficient and the mesh size provides further support for the hypothesis that mesh refinement can, in some cases, negatively affect the results.

- The importance of the input parameters can change depending on the hydrological conditions. Under the low-intensity precipitation (level 1), the roughness parameter is affecting the results more than other parameters. Whereas, under moderate and high-intensity precipitations (levels 2 and 3), the runoff coefficient is the most influencing parameter, which corresponds to the higher variation in outputs.

ACKNOWLEDGEMENTS

DATA REFERENCE

The data used in this work including precipitation data and measured discharge data are available at http://www.senorge.no/. The Digital Terrain Models and land cover maps are acquired from https://hoydedata.no/LaserInnsyn/ and https://land.copernicus.eu/pan-european/corine-land-cover, respectively. The Taguchi and ANOVA analyses were implemented using the Minitab 19 software.

DATA AVAILABILITY STATEMENT

All relevant data are included in the paper or its Supplementary Information.

REFERENCES

Abily, M., Delestre, O., Gourbesville, P., Bertrand, N., Duluc, C.-M. & Richet, Y. 2016 Global sensitivity analysis with 2D hydraulic codes: application on uncertainties related to high-resolution topographic data, Advances in Hydroinformatics. Springer, Berlin, pp. 301–315. https://doi.org/10.1007/978-981-287-615-7_21.

Ahmadisharaf, E., Kalyanapu, A. J. & Bates, P. D. 2018 A probabilistic framework for floodplain mapping using hydrological modeling and unsteady hydraulic modeling. Hydrological Sciences Journal 63(12), 1759–1775. https://doi.org/10.1080/02626667.2018.1525615.

Arcement, G. J. & Schneider, V. R. 1989 Guide for selecting Manning's roughness coefficients for natural channels and flood plains. US Government Printing Office Washington, DC. https://doi.org/10.3133/wsp2339.

Bao, Z., Yang, F., Wu, Z., Nyamsi, S. N. & Zhang, Z. 2013 Optimal design of metal hydride reactors based on CFD -Taguchi combined method. Energy Conversion and Management, 65, 322–330. https://doi.org/10.1016/j.enconman.2012.07.027.

Bellos, V., Papageorgaki, I., Kourtis, I., Vangelis, H., Kalogiros, I. & Tsakiris, G. 2020 Reconstruction of a flash flood event using a 2D hydrodynamic model under spatial and temporal variability of storm. Natural Hazards: 1–16. https://doi.org/10.1007/s11069-020-03891-3.

Bomers, A., Schielen, R. M. J. & Hulscher, S. J. 2019 The influence of grid shape and grid size on hydraulic river modelling performance. Environmental fluid mechanics, 19(5), 1273–1294.

Campolongo, F., Saltelli, A. & Cariboni, J. 2011 From screening to quantitative sensitivity analysis. A unified approach. Computer Physics Communications, 182(4), 978–988. https://doi.org/10.1016/j.cpc.2010.12.039.

Caviedes-Voullième, D., García-Navarro, P. & Murillo, J. 2012 Influence of mesh structure on 2D full shallow water equations and SCS Curve Number simulation of rainfall/runoff events. Journal of hydrology, 448, 39–59.

Chen, B., Krajewski, W. F., Helmers, M. J. & Zhang, Z. 2019 Spatial variability and temporal persistence of event runoff coefficients for cropland hillslopes. Water Resources Research, 55(2), 1583–1597.

Chen, S., Garambois, P.-A., Finaud-Guyot, P., Dellinger, G., Mose, R., Terfous, A. & Ghenaim, A. 2018 Variance based sensitivity analysis of 1D and 2D hydraulic models: An experimental urban flood case. Environmental Modelling & Software, 109, 167–181. https://doi.org/10.1016/j.envsoft.2018.08.008.

Conde, D. A., Canelas, R. B. & Ferreira, R. M. 2020 A unified object-oriented framework for CPU+ GPU explicit hyperbolic solvers. Advances in Engineering Software, 148, 102802. https://doi.org/10.1016/j.advengsoft.2020.102802.

Conde, D. A., Telhado, M. J., Baptista, M. A. V. & Ferreira, R. M. 2015 Severity and exposure associated with tsunami actions in urban waterfronts: the case of Lisbon, Portugal. Natural Hazards, 79(3), 2125–2144. https://doi.org/10.1007/s11069-015-1951-z.

Costabile, P. & Costanzo, C. 2021 A 2D-SWEs framework for efficient catchment-scale simulations: Hydrodynamic scaling properties of river networks and implications for non-uniform grids generation. *Journal of Hydrology*, **599**, 126306.

Dorn, H., Vetter, M. & Höfle, B. 2014 GIS-based roughness derivation for flood simulations: a comparison of orthophotos, LiDAR and crowdsourced geodata. *Remote sensing*, **6**(2), 1739–1759. https://doi.org/10.3390/rs6021739.

Dottori, F., Di Baldassarre, G. & Todini, E. 2013 Detailed data is welcome, but with a pinch of salt: Accuracy, precision, and uncertainty in flood inundation modeling. *Water Resources Research*, **49**(9), 6079–6085. https://doi.org/10.1002/wrcr.20406.

Fanchi, J. R. 2005 *Principles of applied reservoir simulation*. Elsevier, Oxford. https://doi.org/10.1016/C2017-0-00352-X.

Fernández-Pato, J., Caviedes-Voullième, D. & García-Navarro, P. 2016 Rainfall/runoff simulation with 2D full shallow water equations: Sensitivity analysis and calibration of infiltration parameters. *Journal of Hydrology*, **536**, 496–513. https://doi.org/10.1016/j.jhydrol.2016.03.021.

Ferraro, D., Costabile, P., Costanzo, C., Petaccia, G. & Macchione, F. 2020 A spectral analysis approach for the a priori generation of computational grids in the 2-D hydrodynamic-based runoff simulations at a basin scale. *Journal of Hydrology*, **582**, 124508.

Ferreira, R. M., Franca, M. J., Leal, J. G. & Cardoso, A. H. 2009 Mathematical modelling of shallow flows: Closure models drawn from grain-scale mechanics of sediment transport and flow hydrodynamics. *Canadian journal of civil engineering*, **36**(10), 1605–1621. https://doi.org/10.1139/L09-033.

Geuzaine, C. & Remacle, J. F. 2009 Gmsh: A 3-D finite element mesh generator with built-in pre-and post-processing facilities. *International journal for numerical methods in engineering*, **79**(11), 1309–1331. https://doi.org/10.1002/nme.2579.

Ghasemizade, M., Baroni, G., Abbaspour, K. & Schirmer, M. 2017 Combined analysis of time-varying sensitivity and identifiability indices to diagnose the response of a complex environmental model. *Environmental Modelling & Software*, **88**, 22–34. https://doi.org/10.1016/j.envsoft.2016.10.011.

Gibson, M. J., Savic, D. A., Djordjevic, S., Chen, A.S., Fraser, S. & Watson, T. 2016 Accuracy and computational efficiency of 2D urban surface flood modelling based on cellular automata. *Procedia Engineering*, **154**, 801–810.

Hadi, M. N., Farhan, N. A. & Sheikh, M. N. 2017 Design of geopolymer concrete with GGBFS at ambient curing condition using Taguchi method. *Construction and Building Materials*, **140**, 424–431. https://doi.org/10.1016/j.conbuildmat.2017.02.131.

Hu, R., Fang, F., Salinas, P. & Pain, C. 2018 Unstructured mesh adaptivity for urban flooding modelling. *Journal of hydrology*, **560**, 354–363.

Hu, R., Fang, F., Salinas, P., Pain, C., Domingo, N. S. & Mark, O. 2019 Numerical simulation of floods from multiple sources using an adaptive anisotropic unstructured mesh method. *Advances in Water Resources*, **123**, 173–188. https://doi.org/10.1016/j.advwatres.2018.11.011.

Kacker, R. N., Lagergren, E. S. & Filliben, J. J. 1991 Taguchi's orthogonal arrays are classical designs of experiments. *Journal of research of the National Institute of Standards and Technology*, **96**(5), 577. https://dx.doi.org/10.6028%2Fjres.096.034.

Karmakar, B., Dhawane, S. H. & Halder, G. 2018 Optimization of biodiesel production from castor oil by Taguchi design. *Journal of Environmental Chemical Engineering*, **6**(2), 2684–2695. https://doi.org/10.1016/j.jece.2018.04.019.

Khang, D. S., Tan, R. R., Uy, O. M., Promentilla, M. A. B., Tuan, P. D., Abe, N. & Razon, L. F. 2017 Design of experiments for global sensitivity analysis in life cycle assessment: the case of biodiesel in Vietnam. *Resources, Conservation and Recycling*, **119**, 12–23. https://doi.org/10.1016/j.resconrec.2016.08.016.

Kim, B., Sanders, B. F., Schubert, J. E. & Famiglietti, J. S. 2014 Mesh type tradeoffs in 2D hydrodynamic modeling of flooding with a Godunov-based flow solver. *Advances in Water Resources*, **68**, 42–61.

LeVeque, R. J. 2002 Finite volume methods for hyperbolic problems, 31. Cambridge university press, Cambridge. 10.1017/CBO9780511791253.

Lim, N. J. & Brandt, S. A. 2019 Flood map boundary sensitivity due to combined effects of DEM resolution and roughness in relation to model performance. *Geomatics, Natural Hazards and Risk*, **10**(1), 1613–1647. https://doi.org/10.1080/19475705.2019.1604573.

Mejia, A. I. & Reed, S. 2011 Evaluating the effects of parameterized cross section shapes and simplified routing with a coupled distributed hydrologic and hydraulic model. *Journal of Hydrology*, **409**(1-2), 512–524. https://doi.org/10.1016/j.jhydrol.2011.08.050.

Merz, R. & Blöschl, G. 2009 A regional analysis of event runoff coefficients with respect to climate and catchment characteristics in Austria. *Water Resources Research*, **45**(1), W01405. https://doi.org/10.1029/2008WR007163.

Merz, R., Blöschl, G. & Parajka, J. 2006 Spatio-temporal variability of event runoff coefficients. *Journal of Hydrology*, **331**(3-4), 591–604.

Murray, P. M., Bellany, F., Benhamou, L., Bučar, D.-K., Tabor, A. B. & Sheppard, T. D. 2016 The application of design of experiments (DoE) reaction optimisation and solvent selection in the development of new synthetic chemistry. *Organic & Biomolecular Chemistry*, **14**(8), 2373–2384. https://doi.org/10.1039/C5OB01892G.

Neal, J. C., Odoni, N. A., Trigg, M. A., Freer, J. E., Garcia-Pintado, J., Mason, D. C., Wood, M. & Bates, P. D. 2015 Efficient incorporation of channel cross-section geometry uncertainty into regional and global scale flood inundation models. *Journal of Hydrology*, **529**, 169–183. https://doi.org/10.1016/j.jhydrol.2015.07.026.

Papaioannou, G., Vasiliades, L., Loukas, A. & Aronica, G. T. 2017 Probabilistic flood inundation mapping at ungauged streams due to roughness coefficient uncertainty in hydraulic modelling. *Advances in Geosciences*, **44**, 23. https://doi.org/10.5194/adgeo-44-23-2017.

Pappenberger, F., Beven, K., Horritt, M. & Blazkova, S. J. J. O. H. 2005 Uncertainty in the calibration of effective roughness parameters in HEC-RAS using inundation and downstream level observations. **302**(1-4), 46–69. https://doi.org/10.1016/j.jhydrol.2004.06.036.

Park, Y., Cho, K. H., Kang, J.-H., Lee, S. W. & Kim, J. H. 2014 Developing a flow control strategy to reduce nutrient load in a reclaimed multi-reservoir system using a 2D hydrodynamic and water quality model. *Science of the total environment*, **466**, 871–880. https://doi.org/10.1016/j.scitotenv.2013.07.041.

Pianosi, F., Beven, K., Freer, J., Hall, J. W., Rougier, J., Stephenson, D. B. & Wagener, T. 2016 Sensitivity analysis of environmental models: A systematic review with practical workflow. *Environmental Modelling & Software*, **79**, 214–232. https://doi.org/10.1016/j.envsoft.2016.02.008.

Plackett, R. L. & Burman, J. P. 1946 The design of optimum multifactorial experiments. *Biometrika*, **33**(4), 305–325.

Rao, C. R. 1947 Factorial experiments derivable from combinatorial arrangements of arrays. *Supplement to the Journal of the Royal Statistical Society*, **9**(1), 128–139. https://doi.org/10.2307/2983576.

Rao, R. S., Prakasham, R., Prasad, K. K., Rajesham, S., Sarma, P. & Rao, L. V. 2004 Xylitol production by Candida sp.: parameter optimization using Taguchi approach. *Process Biochemistry*, **39**(8), 951–956. https://doi.org/10.1016/S0032-9592(03)00207-3.

Ross, P. J. & Ross, P. J. 1988 *Taguchi techniques for quality engineering: loss function, orthogonal experiments, parameter and tolerance design*. McGraw-Hill, New York.

Sadeghi, S. H., Moosavi, V., Karami, A. & Behnia, N. 2012 Soil erosion assessment and prioritization of affecting factors at plot scale using the Taguchi method. *Journal of Hydrology*, **448**, 174–180. https://doi.org/10.1016/j.jhydrol.2012.04.038.

Sadrzadeh, M. & Mohammadi, T. 2008 Sea water desalination using electrodialysis. *Desalination*, **221**(1-3), 440–447. https://doi.org/10.1016/j.desal.2007.01.103.

Sauer, A. & Ortlepp, R. 2021 Parameter uncertainties in flood hazard analysis of heavy rain events. *ASCE-ASME Journal of Risk and Uncertainty in Engineering Systems, Part A: Civil Engineering*, **7**(2), 04021016.

Savage, J., Pianosi, F., Bates, P., Freer, J. & Wagener, T. 2016 Quantifying the importance of spatial resolution and other factors through global sensitivity analysis of a flood inundation model. *Water Resources Research*, **52**(11), 9146–9163. https://doi.org/10.1002/2015WR018198.

Schubert, J. E., Sanders, B. F., Smith, M. J. & Wright, N. G. 2008 Unstructured mesh generation and landcover-based resistance for hydrodynamic modeling of urban flooding. *Advances in Water Resources*, **31**(12), 1603–1621. https://doi.org/10.1016/j.advwatres.2008.07.012.

Schumann, G., Matgen, P., Hoffmann, L., Hostache, R., Pappenberger, F. & Pfister, L. 2007 Deriving distributed roughness values from satellite radar data for flood inundation modelling. *Journal of Hydrology*, **344**(1-2), 96–111. https://doi.org/10.1016/j.jhydrol.2007.06.024.

Song, X., Zhang, J., Zhan, C., Xuan, Y., Ye, M. & Xu, C. J. 2015 Global sensitivity analysis in hydrological modeling: Review of concepts, methods, theoretical framework, and applications. **523**, 739–757. https://doi.org/10.1016/j.jhydrol.2015.02.013.

Stahle, L. & Wold, S. 1989 Analysis of variance (ANOVA). *Chemometrics and intelligent laboratory systems*, **6**(4), 259–272. https://doi.org/10.1016/0169-7439(89)80095-4.

Subramanya, K. 2013 *Engineering Hydrology*, 4e. Tata McGraw-Hill Education, New Delhi, India.

Taguchi, G., Organization, A. P. & productivité, O. 1986 *Introduction to Quality Engineering: Designing Quality Into Products and Processes*. Asian productivity Organization Tokyo.

Teng, J., Jakeman, A .J., Vaze, J., Croke, B. F., Dutta, D. & Kim, S. J. E. M., Software, 2017. Flood inundation modelling: A review of methods, recent advances and uncertainty analysis. **90**, 201–216. https://doi.org/10.1016/j.envsoft.2017.01.006.

Tian, W. 2013 A review of sensitivity analysis methods in building energy analysis. *Renewable and Sustainable Energy Reviews*, **20**, 411–419. https://doi.org/10.1016/j.rser.2012.12.014.

van Griensven, A. v., Meixner, T., Grunwald, S., Bishop, T., Diluzio, M. & Srinivasan, R. 2006 A global sensitivity analysis tool for the parameters of multi-variable catchment models. *Journal of hydrology*, **324**(1-4), 10–23. https://doi.org/10.1016/j.jhydrol.2005.09.008.

van Vuren, S., Paarlberg, A. & Havinga, H. 2015 The aftermath of 'Room for the River' and restoration works: Coping with excessive maintenance dredging. *Journal of hydro-environment research*, **9**(2), 172–186. https://doi.org/10.1016/j.jher.2015.02.001.

Viglione, A., Merz, R. & Blöschl, G. 2009 On the role of the runoff coefficient in the mapping of rainfall to flood return periods. *Hydrology and Earth System Sciences*, **13**(5), 577–593.

Vojtek, M., Petroselli, A., Vojteková, J. & Asgharinia, S. 2019 Flood inundation mapping in small and ungauged basins: sensitivity analysis using the EBA4SUB and HEC-RAS modeling approach. *Hydrology Research*, **50**(4), 1002–1019. https://doi.org/10.2166/nh.2019.163.

Wang, C., Li, Y. & Huang, G. 2017 Taguchi-factorial type-2 fuzzy random optimization model for planning conjunctive water management with compound uncertainties. *Environmental modelling & software*, **97**, 184–200. https://doi.org/10.1016/j.envsoft.2017.08.007.

Werner, M., Hunter, N. & Bates, P. 2005 Identifiability of distributed floodplain roughness values in flood extent estimation. *Journal of Hydrology*, **314**(1-4), 139–157. https://doi.org/10.1016/j.jhydrol.2005.03.012.

Whitford, W. G., Lundgren, M. & Fairbank, A. 2018 *Cell Culture Media in Bioprocessing, Biopharmaceutical Processing*. Elsevier, Oxford, pp. 147–162. https://doi.org/10.1016/B978-0-08-100623-8.00008-6.

Xing, Y., Shao, D., Ma, X., Zhang, S. & Jiang, G. 2021 Investigation of the importance of different factors of flood inundation modeling applied in urbanized area with variance-based global sensitivity analysis. *Science of The Total Environment*, **772**, 145327.

Yang, J. 2011 Convergence and uncertainty analyses in Monte-Carlo based sensitivity analysis. *Environmental Modelling & Software*, **26**(4), 444–457. https://doi.org/10.1016/j.envsoft.2010.10.007.

Yang, W. p. & Tarng, Y. 1998 Design optimization of cutting parameters for turning operations based on the Taguchi method. *Journal of materials processing technology*, **84**(1-3), 122–129. https://doi.org/10.1016/S0924-0136(98)00079-X.

Yu, D. & Lane, S. N. 2006 Urban fluvial flood modelling using a two-dimensional diffusion-wave treatment, part 1: mesh resolution effects. *Hydrological Processes: An International Journal*, **20**(7), 1541–1565. https://doi.org/10.1002/hyp.5935.

Yuangyai, C. & Nembhard, H. B. 2015 *Chapter 8 - Design of experiments: A key to innovation in nanotechnology*. In: Ahmed, W., Jackson, M.J. (Eds.), Emerging Nanotechnologies for Manufacturing (Second Edition). William Andrew Publishing, Boston, pp. 230–254. https://doi.org/10.1016/B978-0-323-28990-0.00008-7.

Zadeh, F. K., Nossent, J., Sarrazin, F., Pianosi, F., van Griensven, A., Wagener, T. & Bauwens, W. 2017 Comparison of variance-based and moment-independent global sensitivity analysis approaches by application to the SWAT model. *Environmental Modelling & Software*, **91**, 210–222. https://doi.org/10.1016/j.envsoft.2017.02.001.

Zhang, T., Feng, P., Maksimović, Č. & Bates, P. D. 2016 Application of a three-dimensional unstructured-mesh finite-element flooding model and comparison with two-dimensional approaches. *Water resources management*, **30**(2), 823–841. https://doi.org/10.1007/s11269-015-1193-6.

Zischg, A. P., Felder, G., Weingartner, R., Quinn, N., Coxon, G., Neal, J., Freer, J. & Bates, P. 2018a Effects of variability in probable maximum precipitation patterns on flood losses. Hydrology and earth system sciences, **22**(5), 2759–2773. https://doi.org/10.5194/hess-22-2759-2018.

Zischg, A. P., Mosimann, M., Bernet, D. B. & Röthlisberger, V. 2018b Validation of 2D flood models with insurance claims. *Journal of hydrology*, **557**, 350–361. https://doi.org/10.1016/j.jhydrol.2017.12.042.